IEEE Access
Multidisciplinary | Rapid Review | Open Access Journal

Received 5 September 2023, accepted 7 September 2023, date of publication 18 September 2023,
date of current version 27 September 2023.

Digital Object Identifier 10.1109/ACCESS.2023.3316708

RESEARCH ARTICLE

PKC-RCM: Preoperative Kinematic Calibration for Enhancing RCM Accuracy in Automatic Vitreoretinal Robotic Surgery

ALIREZA ALIKHANI[1], (Graduate Student Member, IEEE), SATOSHI INAGAKI[1,2], JUNJIE YANG[1], SHERVIN DEHGHANI[3], (Graduate Student Member, IEEE), MICHAEL SOMMERSPERGER[3], (Graduate Student Member, IEEE), KAI HUANG[4], (Member, IEEE), MATHIAS MAIER[1], NASSIR NAVAB[3], AND M. ALI NASSERI[1], (Member, IEEE)

[1]Augenklinik und Poliklinik, Klinikum rechts der Isar der Technische Universität München, 81675 Munich, Germany
[2]NSK Ltd., Shinagawa-ku 141-8560, Japan
[3]Department of Computer Science, Technische Universität München, 85748 Munich, Germany
[4]Laboratory of Machine Intelligence and Advanced Computing, Sun Yat-sen University, Guangzhou 510275, China

Corresponding author: Alireza Alikhani (alireza.alikhani@tum.de)

This work was supported in part by NSK Ltd., Japan; and in part by the state of the Bavaria through Bayerische Forschungsstiftung (BFS) under Grant AZ-1503-21-BiRoMicO.

ABSTRACT Many robotic systems have emerged in the recent past as cutting-edge solutions to enhance the capabilities of ophthalmic surgeons in order not only to increase the quality of conventional operations but also to enable new and advanced interventions such as gene- and stem-cell-based therapies. Some of these operations require precise and stable delivery of therapeutics into the sub-retinal domain and therefore, automatic procedures with micron precision at the tooltip are essential. One of the most critical parameters to precisely maintain the tooltip in automated robotic retinal surgery is the appropriate configuration and control of the Remote Center of Motion (RCM). The RCM precision might be affected by any physical uncertainties, such as instrument assembling, or minor kinematic changes. Therefore, an accurate RCM identification requires an extensive calibration plan before each operation. This paper presents a novel preoperative evaluation-calibration method for kinematic-adjustable software-based RCM robots. Our key concept is decomposing the 3D workspace into two orthogonal working planes in order to reduce the complexity while adding robustness to RCM evaluation and software calibration. First, we propose an ablation-based RCM-related analysis method of the kinematics of the robot. Using a Convolutional Neural Network (CNN), we analyze image-based RCM along the instrument during a predefined RCM motion maneuver. Utilizing software calibration protocol by prior-analyzed RCM-related kinematic parameters, the software calibration is done automatically. The process is repeated until the RCM accuracy is set within a clinically acceptable range. Evaluation of the method on a highly accurate 5-DOF-Software-RCM robot demonstrated significant optimization in RCM error within an average of 4 minutes for each plane and 0.300 ± 0.20 mm accuracy.

INDEX TERMS Medical robots and systems, computer vision for medical robotics, surgical robotics, planning, remote center of motion (RCM).

I. INTRODUCTION

The advent of robot-assisted ophthalmic surgical systems has generated substantial clinical interest in recent years, owing to their potential advantages in enhancing the

The associate editor coordinating the review of this manuscript and approving it for publication was Santosh Kumar.

efficacy and safety of ophthalmic procedures. The integration of sophisticated robotic platforms has facilitated the development of innovative therapeutic strategies, enabling ophthalmic surgeons to perform complex surgical procedures with greater precision and accuracy [1], [2], [3], [4], [5]. The deployment of robot-assisted ophthalmic surgical systems has enabled the precise autonomous navigation of surgical instruments through precisely placed trocars on the sclera, typically positioned a minimum of 3.5 mm from the limbus [6]. Constraining the robotic control around the Remote Center of Motion (RCM) during intraocular surgery is imperative to ensure optimal autonomous navigation. There are two main types of RCM mechanisms in robot-assisted ophthalmic surgery systems. Hardware-based-RCM (HRCM) [7] robots with direct physical control over the RCM and straightforward mechanical design of a fixed RCM point along the instrument, ensuring the RCM movement. This mechanism can be reliable, as it is not dependent on the performance of the robotic's kinematic software. On the other hand, its dependency on the mechanical structure provides less flexibility for performing delicate procedures such as orbital manipulation [8], which the surgeon often uses to rotate the eyeball without moving the head.

Software-based-RCM (SRCM) [3] robots rely on computer algorithms and the robot's software to control the position and movement of the RCM with a flexible kinematic inference. SRCM systems can offer this flexibility by updating the RCM through the software. However, physical uncertainties, especially in assembling disposable instruments with diverse geometries lead to misalignment of software parameter from the original values, resulting in RCM and tooltip errors, and adverse outcomes. RCM positioning requirements are reported between 2.5mm and 3.0mm. Gijbels et al. defined a tool tip accuracy of 0.023deg in the XZ and YZ planes and 10um in the Z-Axis (in depth axis) because in the vein cannulation surgeries, the diameter of the vessels is 80um [9]. Moreover, Sakai et al. calculated the tooltip accuracy to be around 15um [10]. Therefore, optimizing the robot's software parameters in the robot's preparation phase and after assembling instruments is critical to ensuring that RCM and tooltip accuracy remain within acceptable ranges and that the proper configuration is maintained. We present a novel pre-operative calibration framework tailored for the use case of SRCM-robot-assisted ophthalmic surgery. The contributions of this work are as follows: **1)**We introduce a robot's kinematic correction protocol based on an ablation scheme applied to the robot software. To discover RCM position-related parameters (RPP) and RCM deviation-related parameters (RDP) in the software, firstly, we decompose the kinematic into two working planes (XZ and YZ), and secondly, we accurately analyze each parameter's impact on the final RCM movement along the needle (Fig. 2 Step: 0). **2)** Using convolutional neural networks (CNNs), we present a robust image-based RCM deviation analysis method during

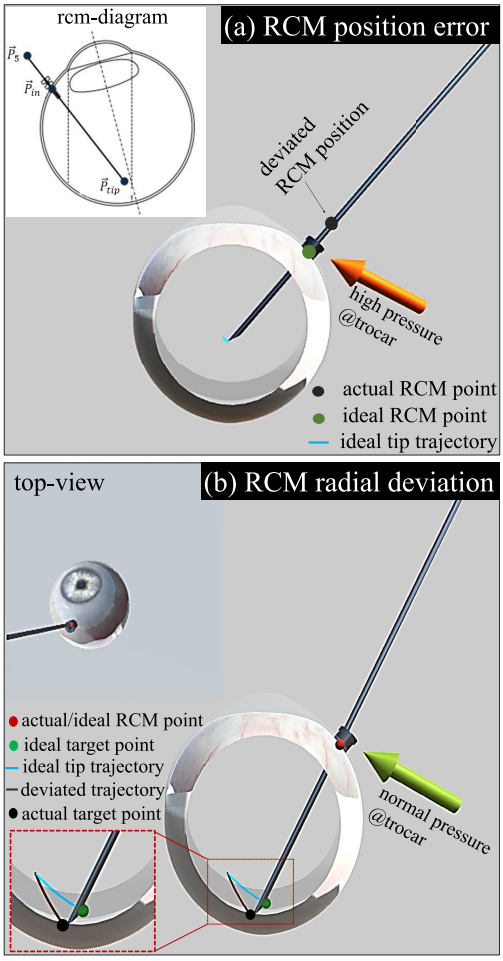

FIGURE 1. Simulated comparison of RCM movement with and without unbalanced robot's software. a- shows the RCM position impact on the tooltip movement. A misaligned RCM position increases undesired pressure on the sclera and reduces the working volume inside the eyeball. b-shows the RCM radial deviation impact on targeting a point. Any movement with unbalanced RDPs can lead the tooltip to an undesired end, making automatic navigation and prediction impossible.

predefined symmetric robot RCM maneuvers in the analyzing planes, as shown in Fig. 2:Step 1-3). We leverage the kinematic analysis to establish a mapping from the kinematic configuration to RCM movements as the reference for parameter adjustment (Fig. 2:Step 4,5). **3)** One of the significant bottlenecks in the utilization of robotic retinal platforms, is the time-consuming preparation process [11], [12]. We introduce a robust RCM calibration method as one of the preparatory steps, which has the potential to reduce the overall time required to prepare these systems significantly. *adjust-test* optimization(Fig. 2:Step 1-5), the RCM-related parameters calibration loop is repeated until the movement converges within an acceptable predefined range of RCM error. Our experiments validate the calibration method on different sub-retinal cannulas controlled by a 5-DoF micro-surgical robot.

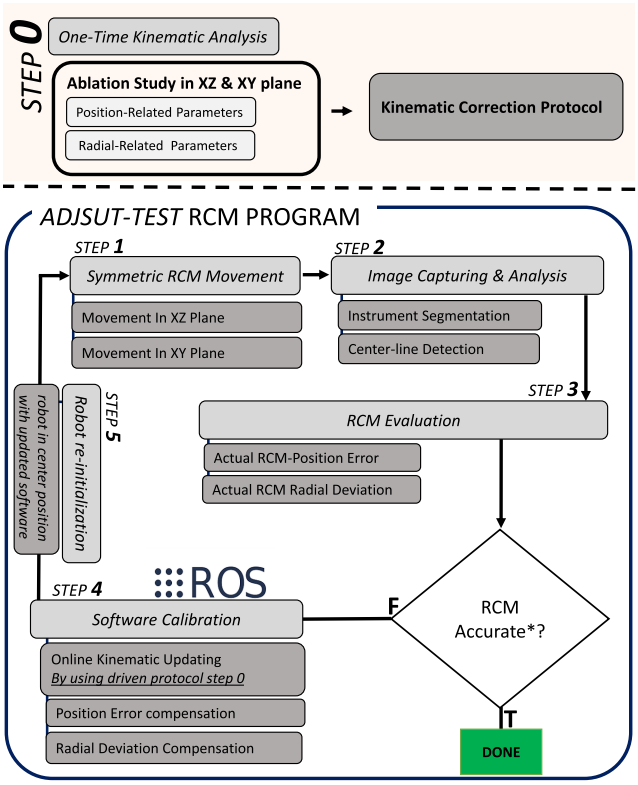

FIGURE 2. The workflow of our method. Initially, the one-time kinematic analysis is done. Then, the "adjust-test" program consisting of RCM movement, RCM evaluation, and Software calibration is executed iteratively. The level of accuracy is defined before the surgery by the surgeon depending on the surgery.

II. RELATED STUDIES

To date, only a few published works share the idea of an autonomous pre-operative SRCM evaluation calibration with previously analyzed RCM-related parameters. Multiple works have focused on RCM position evaluation during surgery using a geometric approach [13], [14], [15]. Some other works involve new modalities to solve the RCM evaluation problem, such as tool-tissue force sensing, static laser tracking, and image-based analysis. Force sensing methods evaluate the performance of RCM movement by integrating force sensors into the shaft of the surgical instruments [14], [16]. Force sensors are commonly used for sensitive measurement of intraoperative extrusion to detect hazardous interactions during tool-tissue interaction. However, combining force feedback with kinematic optimization remains a challenging task. Integrating force sensors into a surgical instrument will introduce a new set of certification and clinical requirements. Laser tracking methods have sufficient precision for capturing a fixed marker in the line of sight [17], [18], whereas these methods require additional mechanical modifications to cover the RCM movement in certain planes. Moreover, these methods require complex and expensive laser devices and extra equipment to be deployed on the surgical platform, which conflicts the pre-operative standard in the operation room. As an alternative, image-based RCM estimation has already been used as a practical solution to evaluate surgical instruments and assessing RCM response [7], [19], [20]. The camera as a standalone module can be easily integrated into the robot system and surgical workflow without affecting the surgical platform. Therefore, numerous research initiatives have been proposed in this area. Conversely, most of the researches are focusing on only RCM position evaluation without kinematic calibration because of dealing with HRCM mechanism.

Rosa et al. [21] implemented a method to estimate the optimal pivoting point (OPP) for mechanical-based RCM laparoscopic surgical robots using a camera system. They extract straight lines from camera images and after removing all outliers by utilizing the RANSAC method, followed a least-squared problem to estimate the optimal incision point of the detected lines. Wilson et al. [22] explore the usage of stereo cameras in the estimation of RCM position during laparoscopic surgeries. These two studies are addressing the RCM position evaluation introspectively on Hardware-based RCM (HRCM) robotic systems. Other proposed methods by [9] and [13] mainly focus on aligning the RCM on the trocar in HRCM robotic platforms. This alignment procedure involves utilizing a calibration tool in order to estimate of optimal pivot position and leveraging the Fulcrum Point in robotic minimally invasive surgeries. Haoran and et al. utilize a method using a stereo cameras and a special distinct marker to detect the instrument and calibrate the robot accordingly for OCT guided retinal surgery, but assembling these markers into a sub-millimeter instruments makes these marker-based methods challenging for preoperative calibration [23].

By contrast, our proposed marker-free method aims not only to detect the RCM position but also to evaluate RCM error and any deviation from the radial movement caused by RCM, eventually leading to the calibration of the robot's software. Secondly, an adjust-test pre-operative iterative program is done to calibrate the SRCM robotics software online using the driven protocol from prior-analyzed kinematics to ensure an accurate RCM motion intraoperatively. Integrating an image-based evaluation method into an existing surgical setup with minor modifications seems promising.

III. METHOD

In this section, we describe our pre-operative RCM evaluation-calibration workflow (Fig. 2) step by step.

A. KINEMATIC ANALYSIS

1) FORWARD AND INVERSE KINEMATICS OF RCM CONTROL

Since software-RCM robots have various mechanical designs, it is essential to analyze their kinematic structures and distinguish critical joints that may cause RCM precision errors. At first, the standard method calculates the forward and inverse kinematics. The forward kinematics of the robot T_j^i is calculated by Denavit–Hartenberg (DH) parameters.

$$T_j^i = A_{i+1}A_{i+2}\ldots A_{j-1}A_j(if\ i < j)$$
$$A_i = R_{z,\theta_i}Trans_{z,d_i}Trans_{x,a_i}R_{x,\alpha_i} \quad (1)$$

where θ_i, a_i, d_i, α_i are parameters associated with link i and joint i. The inverse kinematics is calculated by using the numerical approach (e.g. Jacobian inverse technique) or geometric approach [24], [25]. Second, the RCM control method is calculated. Since the needle needs to pass through the RCM point, the RCM point ($\vec{P}_{in}$) can be denoted as follows [26].

$$\vec{P}_{in} = \vec{P}_5 + \lambda(\vec{P}_{tip} - \vec{P}_5) \tag{2}$$

where $\vec{P}_{tip}$ defines the tip of the instrument and $\vec{P}_5$ defines the endpoint of the robot which can be also defined as the initial point of the instrument as shown in Fig. 1(a-rcm-diagram). From these calculations, SRCM control can be developed.

2) KINEMATIC DECOMPOSITION

The robot software (kinematic) is analyzed separately in two working planes (XZ and YZ plane) to reduce the software analysis complexity. This decomposition enables reducing the number of the related kinematic parameters in each analyzing plane and easier evaluation-calibration using the actual setup, shown in Fig. 3. The kinematic parameters are changed individually to check their impact on the tooltip movement. In the analysis, the RCM point is assumed to be X mm from the tooltip, and RCM rotates the instrument within $\pm\ \theta$ degrees. Two critical RCM parameters are analyzed, RCM position parameters (RPP) and RCM radial parameters (RDP), which cause RCM positioning error and RCM radial deviation, respectively. RCM positioning error means the position of the RCM point is moved away from the intended position (Fig. 1-a), and the RCM radial deviation means the trajectory of the tooltip deviates from the ideal trajectory, which is a circular arc(Fig. 1-b).

From this analysis, the effect of each parameter for RCM movement in each plane is figured out. Knowing this information enables generating an RCM calibration policy.

B. IMAGE CAPTURING/ANALYSIS

Locating two necessary components in each captured frame: the metal cylinder needle and the plastic shoulder, as shown in Fig.4-a. By leveraging the needle pose in each frame, the needle's center line denoting its position and rotation status in the image plane (III-B2) enables RCM-Position extraction along the instrument. Analyzing the radial deviation, we assume the ideal RCM movement has a circular arc trajectory at the tooltip. To achieve a more consistent and reliable trajectory and make the detection method independent from various cannulas geometries at the tooltip, the trajectory of the interconnection point between the needle and shoulder is considered ($Trajec_{shoulder}$) to represent the tooltip trajectory($Trajec_{tip}$). Having shoulder point trajectory after a symmetric RCM maneuver, the radial deviation is analyzed (III-C2).

1) INSTRUMENT SEGMENTATION

A U-Net-style network [28] is trained on a custom dataset with Binary Cross Entropy Loss to obtain the shoulder and

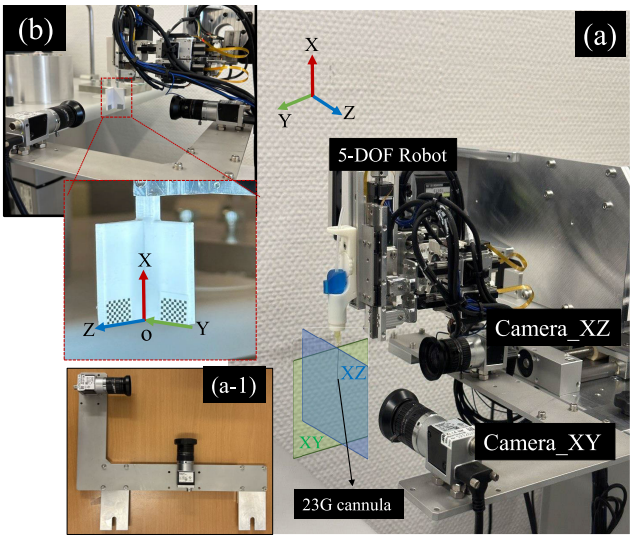

FIGURE 3. (a) - shows the setup containing two cameras mounted on a 90-degree removable handler(a-1) in order to observe all movement in two working planes (XY and XZ) of the robot (5-DOF-SRCM ophthalmic robot). (b) the calibration method of cameras for two planes using a designed 3-printer marker to enable 63-point calibration using Zhang's method [27].

the needle pose in the camera frames (Fig. 4:Step 1). To train the network, we generate a custom dataset containing random positions and orientations of 4 different surgical needles (23G) in two orthogonal planes, manually labeled for surgical needle and its shoulder segmentation. The dataset consists of a training set of 3500 images and a validation set of 350 images.

2) CENTER LINE DETECTION

After extraction of the needle segmentation mask, we fit a 2D line to the segmented needle pixels using Huber Regressor [29]. The line provides the axis line that passes through the center of the needle which is represented as the needle center-line l_c.

3) SHOULDER TRAJECTORY

Having the needle shoulder mask segmented (Fig.4-a) in each frame(III-B1), we utilize the contour detection [30], to contour the shoulder part. To track the connection point of the needle and the plastic shoulder, Fig. 4:Step 3, the intersection of the point on the lower contour's edge and the needle center line (l_c) in each frame is considered as the shoulder point (P_{sh}) reference. The collection of these shoulder points during the RCM movement represents the shoulder trajectory ($Trajec_{shoulder}$).

C. RCM EVALUATION

1) EXTRACT RCM POSITION

We assume that the RCM position is the point with the least displacement along the needle during the RCM movement. This location is assumed to be the nearest point to all center lines, consistent with the original definition. As shown in

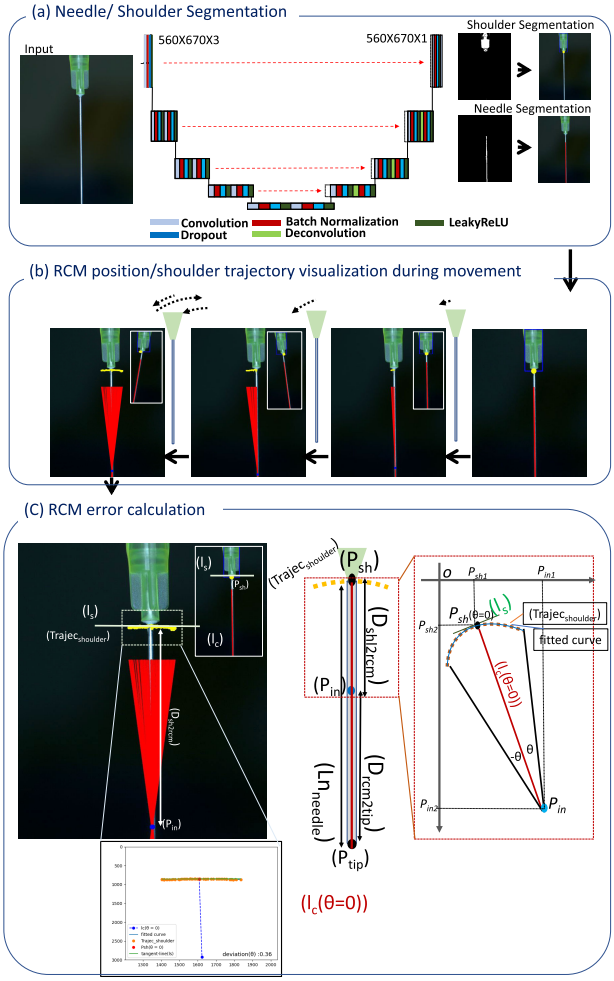

FIGURE 4. Presents the image-based RCM error analysis steps. (a) shows the needle center-line and shoulder-point segmentation using a U-net-style neural network. (b) shows analyzing each frame during the 2-times symmetric RCM movement and visualizes the trajectory. (c) presents the calculation of RCM position and deviation misalignment by utilizing tangent-line passing the shoulder trajectory.

Fig. 4:Step 1, obtaining the center line in each frame during the predefined maneuver enables the calculation of this point. Consequently, the problem of finding the actual RCM point is converted into a least square approximation (Eq. 3) to find the nearest point $\hat{P}_{in}$ for all k 2-dimensional needle center-lines extracted from the previous section. Each center line is characterized by a point a and a direction $\vec{n}$ [31].

$$\begin{aligned}\hat{P}_{in} &= \underset{p}{\operatorname{argmin}}\ Dist\ (p; A, N)\\ &= \underset{p}{\operatorname{argmin}} \sum_{j=1}^{K} Dist\ \left(p; a_j, \vec{n}_j\right)\\ &= \underset{p}{\operatorname{argmin}} \sum_{j=1}^{K} \left(a_j - p\right)^T - \left(I - \vec{n}_j \vec{n}_j^T\right)\left(a_j - p\right) \end{aligned} \quad (3)$$

At this stage, we need to calculate the length between the RCM position and needle tip ($Dist_{rcm2tip}$). Having the calculated Euclidean distance between RCM position (P_{in}) and Shoulder point (P_{sh}) with a known needle length (Len_{needle}), the number of pixels showing RCM position from the tooltip is calculated as shown in Fig. 4-(c). By having the pixel size (Pxl_{size}), the RCM position in mm is extracted. We calculate the RCM position with respect to the tooltip, as shown in Eq. 4.

$$\begin{aligned} Dist &= |P_{in} - P_{sh}| \times Pxl_{size}\\ Dist_{rcm2tip} &= |Len_{needle} - Dist| \end{aligned} \quad (4)$$

2) EXTRACT RCM RADIAL DEVIATION

The tangent line to a circle at a point on the circle is perpendicular to the radius to that point [32]. Then as mentioned in III-B1, based on RCM definition, the trajectory of the tooltip and shoulder in a symmetric ideal RCM movement from $[-\theta, \theta]$ should result in an arc, with the RCM point being its center. Therefore the tangent line that passes a point on this trajectory ($P_{sh}(\theta = 0)$) is perpendicular to the line that connects this point and analyzed RCM (P_in), described in III-C1. Having this theory, any deviation from perpendicularity is considered as the RCM radial deviation(Fig. 4:Step 3). To calculate this deviation, after collecting the shoulder trajectory points in the symmetric predefined RCM maneuver (III-B3, we construct the best curve fit (fitted curve) to the extracted points by using polynomial regression method [33]. Thereafter, the tangent line l_c passes from $P_{sh}(\theta = 0)$ is calculated, shown as Step:3 of Fig. 4.

$$\begin{aligned} l_c &= m_{l_c} \times x + y0\\ deg_{m_{l_c}} &= \arctan(m_{l_c})\\ \frac{dy}{dx}(Dist(sh2rcm)) &= \frac{y_{P_sh} - y_{P_in}}{x_{P_sh} - x_{P_in}}\\ deg_{Dist(sh2rcm)} &= \arctan(\frac{dy}{dx}(Dist_{sh2rcm})) \end{aligned} \quad (5)$$

As presented in Equation (5), the next step is the calculation of slopes and angles of two lines, m_{l_c}, $deg_{m_{l_c}}$, $\frac{dy}{dx}(Dist(sh2rcm))$, and $deg_{Dist(sh2rcm)}$ and compare the difference in angles with the ideal RCM movement angle which is 90 degree.

$$deviation = | \ (deg_{Dist(sh2rcm)} - deg_{m_{l_c}}) - 90 \ |_{ideal=90} \quad (6)$$

Analyzing the driven slope (m) of the fitted line w.r.t the perpendicular line connecting the shoulder point and the RCM point in analyzing frame indicates the deviation factor. Figure 5 shows how the RCM position and radial deviation are calculated with different software parameters in comparison with kinematic theoretical analysis.

IV. EXPERIMENTS

In this section, we focus on the 5-DoF ophthalmic surgical robot, shown in Fig. 3. Furthermore, to generalize the method for utilizing it in other SRCM robots, we conducted the kinematic analysis on an industrial 6-DOF arm robot (VS060, DENSO Corporation), described in IV-A2.

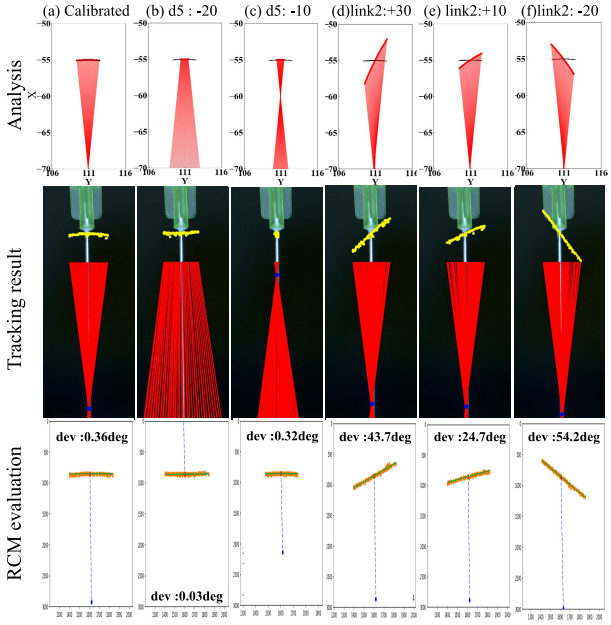

FIGURE 5. RCM evaluation with different software parameters in 5-DoF-SRCM ophthalmic robot described in IV-A1 in XZ plane. A comparison between the theoretical analysis of the software as a ground truth and our proposed method is presented. The calibrated parameters for d_5 and $link_2$ are 65.9 and 47 mm respectively.

A. KINEMATIC ANALYSIS

1) 5-DOF SURGICAL ROBOT

Our 5-DoF surgical robot is presented in Fig. 6, which is an updated version of the model proposed by Nasseri et al. [3], prototyped by NSK.Ltd. The robot consists of two parallel coupled joint mechanisms (PCJM) for translation and rotation in the Z and Y axis, and a decoupled prismatic joint for the movement along the X axis. All five linear actuators are driven by corresponding ball-screw step motors with improved holding force and stability. The coordinated movement of the parallel actuator couple defines the length of the corresponding transnational joint. Meanwhile, the length difference of two parallel actuators is converted into a virtual revolute joint. Referring to the kinematic structure in Fig. 6, we obtain the needle-tip position $P_{tip} = [p_x\ p_y\ p_z]^T$ (Eq. 7), by forward kinematics where o_j, l_j, $\dot{c}_j$ and $\dot{s}_j$ are the abbreviations of $offset_j$, $link_j$, $cos(\theta_j)$ and $sin(\theta_j)$ respectively.

$$\begin{aligned} p_x &= (-d_5\dot{c}_4 - l_2\dot{s}_2 - o_1)\dot{c}_2 + (l_1 - o_2)\dot{s}_2 \\ p_y &= d_3 - d_5\dot{s}_4 + l_2\dot{c}_4 \\ p_z &= d_1 + (d_5\dot{c}_4 + l_2\dot{s}_4 + o_1)\dot{s}_2 + (l_1 - o_2)\dot{c}_2 \end{aligned} \tag{7}$$

Since the position of the RCM point varies in vitreoretinal surgery, in this paper we set this point (P_{rcm}) at 20 mm from the tip along the needle, and control our robot to move around this point by utilizing Eq. 2.

The parallel actuators are responsible for both translational and rotational movements, and each actuator is measured by its accurate linear encoder and controlled in a closed loop. We assume that the two virtual revolute joints θ_2 and

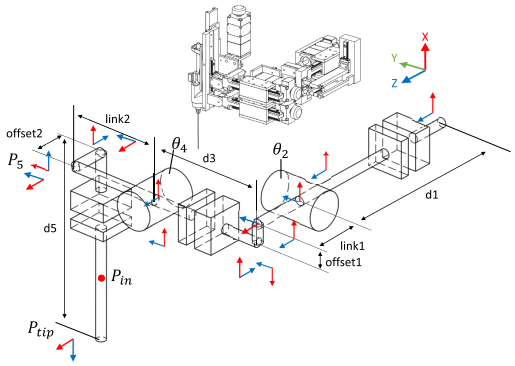

FIGURE 6. The kinematic structure of the 5-DoF ophthalmic surgical robot.

θ_4 are precise enough to avoid a calibration deadlock. Knowing the relationship between the tip position and each joint, we first analyze how the RCM precision error can be ideally generated from the error of certain joints. From Eq. 7, d_1 and d_3 are transnational parameters and never interfere with the RCM movement. Besides that, $offset_2$ and $link_1$ can be considered as one parameter, being always utilized jointly. In summary, $offset_1$, ($offset_2$, $link_1$), $link_2$, and d_5 are the only parameters responsible for the RCM movement. Furthermore, considering the calibration before the surgery, d_5, $link_2$, and $offset_2$, these three parameters can be misaligned by assembling a new cannula and must be calibrated(see Fig. 6). In the next step, let's consider that each parameter has an initial +5 mm offset, and calculate the theoretical needle-tip trajectory. This calculation simulates the behavior when the actual parameters have errors relative to the design values. We calculated the trajectory of the instrument as shown in Fig. 7. The graphs show the effect of the three parameters(d_5, $link_2$, and $offset_2$) related to the instrument's replacement.

In addition to the three parameters, the effect of all kinematic parameters is summarised in Table. 1. The RCM position in XZ and XY is directly affected by d_5 and $offset_1$. We call this error as **RCM-position error** and the set of d_5 and $offset_1$ as **position-related parameters**. The RCM radial movement is directly affected by parameters $offset_2$ and $link_2$. In this case, the RCM position is not shifted, but the radial movement of the tip has completely deviated. We call this RCM error, **RCM radial deviation** and set of $offset_2$ and $link_2$ parameters as **deviation-related parameters**.

According to the analysis result in this table, we separate the evaluation of RCM movement in two orthogonal planes as XZ and XY, since RCM movement in XZ and XY is entirely independent of the kinematic parameters, respectively.

2) 6-DOF ROBOT ARM

The kinematic structure of the 6-DOF arm robot(VS060, DENSO Corporation) is shown in Fig. 8, and the instrument is attached to the end of the robot arm. The first step is the decomposition of the kinematics into two orthogonal planes

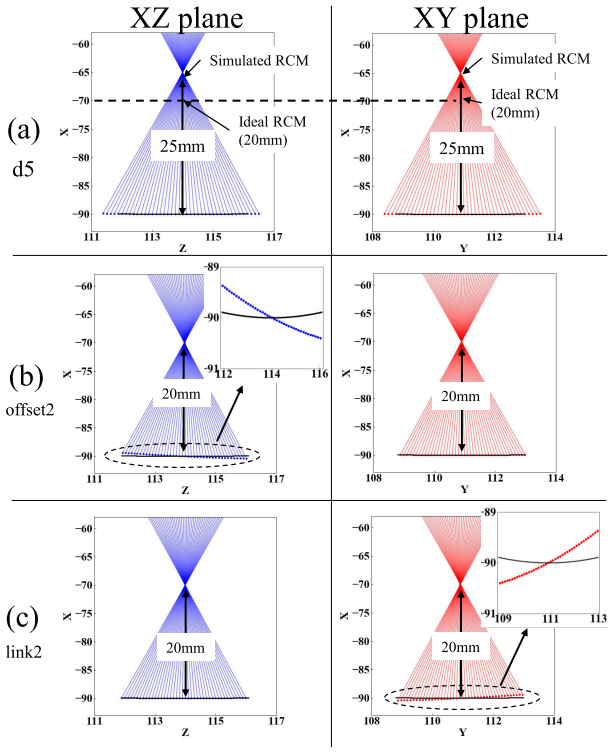

FIGURE 7. RCM analysis of 5-DoF surgical robot in *XZ* and *XY* by changing the kinematic parameters. The RCM movement in both planes is analyzed when each parameter is 5mm more than the set value separately. The blue and red areas indicate the area through which the instrument passes, and the black line presents the ideal movement of the tooltip.

TABLE 1. Dependency of RCM Movement of 5-DoF robot. dev and pos represent RDD and RDP respectively. important* shows considered parameters that may be affected by new instrument assembling.

joint	d_1	d_3	d_5	o_1	o_2	l_1	l_2
len (mm)	101	63.1	65.9	4.5	17.7	29.5	49.0
XZ	×	×	pos	pos	dev	dev	×
XY	×	×	pos	×	×	×	dev
important*	×	×	✓	×	✓	×	✓

(XZ and YZ). The RCM movement in these two planes is analyzed as described in III-A1. As shown in Fig. 8, seven parameters need to be considered (d_1-d_7) in this step. In order to examine their impact on the tip movement, each parameter is moved $+5mm$ from the designed value, one by one, and the impact is analyzed as shown in Table. 2.

Same as analyzed 5-DoF robot, these 3 parameters (d_4,d_6,d_7) can be affected by needl's assembly(see Fig. 8). The impact of these 3 parameters is shown in Fig. 9. From this analysis, our analysis method is capable of generating the calibration protocol for other SRCM robots.

B. SOFTWARE CALIBRATION

As the kinematic analysis explains, RCM motion in each plane is determined by corresponding parameters. The next step is generating a software calibration protocol using this result.

TABLE 2. Dependency of RCM Movement of the 6-DoF robotic arm. dev and pos represent RDD and RDPs respectively and important* shows considered parameters that may be affected by new instrument assembling.

joint	d_1	d_2	d_3	d_4	d_5	d_6	d_7
len (mm)	345	305	300	70	10	50	10
XZ	×	pos	dev	dev	pos	pos	×
YZ	×	×	pos	×	×	pos	dev
important*	×	×	×	✓	×	✓	✓

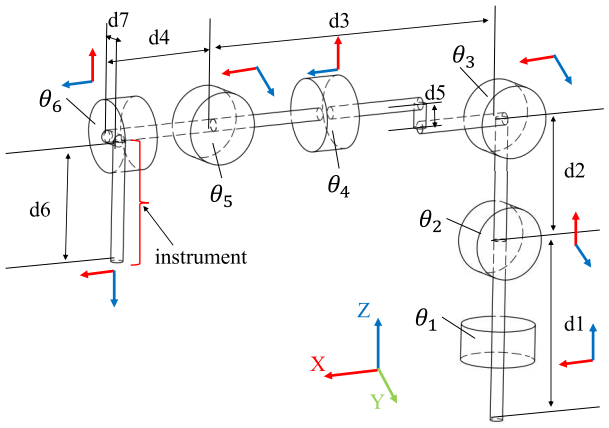

FIGURE 8. The kinematic structure of 6-DoF robot arm.

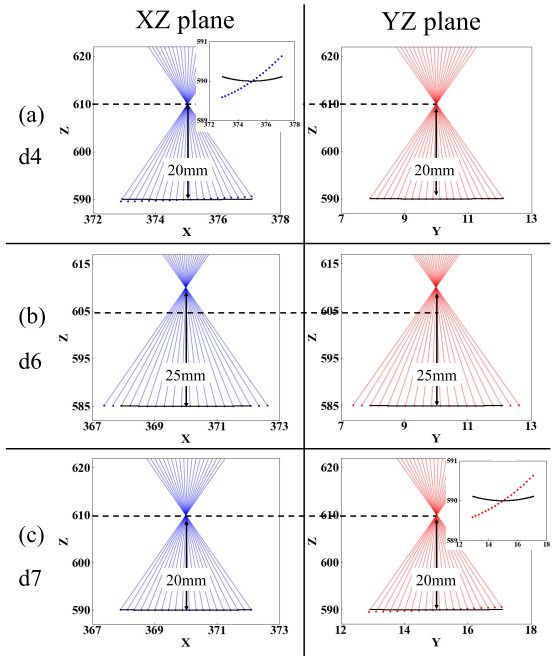

FIGURE 9. RCM analysis of 6-DoF robotic arm in *XZ* and *YZ* by changing the kinematic parameters. The trajectory of the instrument is analyzed in both planes when the actual parameters are 5mm more than the set value separately. The blue and red areas indicate the area through which the instrument passes, and the black line presents the ideal movement of the tooltip.

1) 5-DOF SURGICAL ROBOT

We use the analysis system in Fig. 3 by moving the robot in RCM mode symmetrically by ± 6 degrees two times in two

planes (XY and XZ) separately and follow the rules below to calibrate each RCM plane.

1) If the position of the RCM(P_{xz}) is not at 20 mm(P_{target}) from the tip, adjust $d_5 += P_{target} - P_{xz}$.
2) Check the RCM radial deviation in the XZ and XY plane. If the RCM point has variation, adjust $offset_2$ and $link_2$.
3) Calibration loop will be terminated when RCM position error is within 0.5 mm, and the slope error is within 1 degree. (Due to our robot's technical requirements and surgical setup, we choose these numbers as the RCM requirements to terminate the calibration. The RCM requirement can be set as an input of this method.)

2) 6-DOF ROBOT ARM

The 6-DoF robot arm can also be calibrated by observing two separate planes (XZ and YZ) and following the rules below.

1) If the position of the RCM(P_{xz}) is not at 20 mm(P_{target}) from the tip, adjust $d_6 += P_{target} - P_{xz}$.
2) Check the RCM radial deviation in the XZ and YZ plane. If the RCM point has variation, adjust d_4 and d_7.
3) Calibration loop will be terminated when RCM position error is within 0.5 mm, and the slope error is within 1 degree.

C. IMAGE ACQUISITION AND CAMERA CALIBRATION

For our vision-based calibration approach, we employ two Basler RGB cameras (acA4024-29u), acquiring images at 15 fps with a resolution of 4024 × 3036 pixels. By using a method of Zahng [27], and utilizing a 9 × 7 checkerboard pattern with squares of 1 × 1 mm^2 attached on a 3D-printed calibration part on X-Axis which is shown in Fig.3-b. Cameras are calibrated for both robot planes, and the average calculated pixel size is 0.016 *mm*, and 0.018 *mm* in the XZ and XY planes respectively to be later used in Eq. 4. As the camera is positioned stationary w.r.t to both planes, this calibration is required only once.

D. ANALYSIS OF RCM POSITION DETECTION

In this step, we experimented 15 times misaligned kinematic parameters represented by disassembling and re-assembling a cannula (Geuder G-34285 23G), evaluate the RCM position by our method, and compare the results with the theoretical analysis as a ground truth. As explained in Sec. IV-A1 and shown in Table. 4, three kinematic parameters (d_5, $offset_2$, and $link_2$) can cause RCM errors and are dependent on the needle's assembly. We analyzed the impact of each parameter by on RCM position by our method and compare the results with the theoretical analysis and experiments as depicted in Fig. 10. Each parameter is changed ±2 mm in 1 mm increments from the designed value, and the detected RCM position is investigated. Fig. 10 shows similar behavior in both experimental and theoretical results in the XZ (a), and in the XY(b) planes. The experimental results also confirm that the RCM position is linearly dependent on d_5. The theoretical analysis proves that the RCM position detection is unaffected by changes in the RDPs ($link_2$ and $offest_2$).

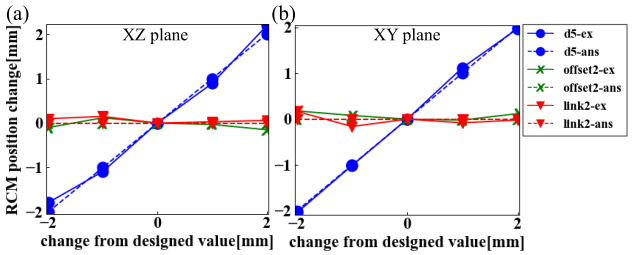

FIGURE 10. The RCM position variation depends on updated kinematic parameters in *XZ* and *XY* planes, respectively. The dashed and solid lines mark the results of the theoretical analysis (ans) and experiments (ex), respectively.

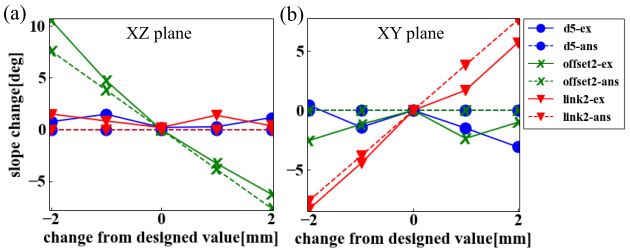

FIGURE 11. The variation in slope of l_c with updated kinematic parameters is shown in the *XZ* and *XY* planes, respectively. The dashed and solid lines correspond to the results of the theoretical analysis (ans) and experiments (ex), respectively.

E. ANALYSIS OF RCM RADIAL DEVIATION

In the following, we evaluate the influence of the kinematic parameters on the RCM radial deviation. Fig. 11 (a) and (b) show the experimental result compared to the expected theoretical values on the XZ and XY plane, respectively. It can be observed that the experiment and theoretical result share the same trend, in which errors from $offset_2$ in the XZ plane and $link_2$ in the XY plane generate RCM radial deviation. The consistency of the results verifies our calibration strategy for $offset_2$ and $link_2$ which is described in IV-B1.

Based on the theoretical analysis driven from Eq.7 and Eq.2 in IV-A1, each degree of radial deviation generates at most ±0.025 mm undesired in-depth movement at the two edges of needle tip during the RCM movement (in our RCM maneuver at ±6 degrees).

F. OVERALL CALIBRATION PERFORMANCE

In the next step, we compared the measured RCM values before and after software calibration with the 5-DoF robot. The average values are shown in Table. 3. In these experiments, we set the RCM point at 20 mm from the tip and used a cannula with a 35 mm length. Therefore, the RCM position distance is expected to be 15 mm from the shoulder point. We also selected an accurate range to terminate the loop (Fig.2) to be ±0.50 mm for RCM position and ±1*degree* for RCM deviation. Before calibration, the average of RCM

TABLE 3. RCM position/deviation before and after calibration.

Task	Position (mm)		Deviation (deg)	
Plane	XZ	XY	XZ	XY
Original	14.21	14.35	-6.70	8.77
Calibrated	14.77	15.12	0.42	0.75

TABLE 4. Designed and the average of calibrated software parameters.

Parameter	d_5	$offset_2$	$link_2$
Original	65.90	17.70	49.00
Calibrated	68.55	15.90	47.58

positions was at 14.21 mm and 14.35 mm on the *XZ* and *XY* plane, respectively. After running the calibration method, the RCM position moved into our defined safe range and was detected at 14.77 mm and 15.12 mm in the *XZ* and *XY* planes. The RCM radial deviation also improved from -6.7 degrees (*XZ*) and 8.77 degrees (*XY*) to 0.42 degrees (*XZ*) and 0.75 degrees (*XY*).

The set of average kinematic parameters corresponding to the improved RCM movement is listed in Table and compared with the designed set of parameters. 4.

In order to have an overview on a tool-tip error during a surgery with/without calibrated RCM, we simulated the behaviour of RCM error and radial deviation, described in IV-A1. Based on these simulations, we calculated the maximum tooltip error in each plane before and after the RCM calibration. The maximum tooltip error (at 6 deg rotation) before calibration is 0.16 mm and 0.241 mm in the XZ and XY planes respectively. The error is improved by 0.085 and 0.018 mm. The proposed method consists of two main parts: RCM evaluation (Fig.2: Step 2-3) and Software Calibration (Fig.2: Step 4). The calibration parts only use driven software calibration protocol and update parameters in real time. We assume that the calibration step does not need to be validated by its definition. On the other hand, the RCM position error and the RCM radial deviation estimation, described in III-B and III-C, can be a potential source of error. Therefore, we design a validation setup, shown in Fig. 12(a), to explicitly validate the RCM evaluation part.

In this validation setup, we utilize a precise stepper motor with a resolution of 0.036 degrees per step, and a 3D-printed circle-shaped stage is attached to the stepper motor. This rotational stage has a groove to hold the needle at the center, and the designed slit perpendicular to the groove helps to detect the stage's center point. The setup rotates ±14 degrees three times to imitate an RCM rotation. In this movement, assuming that the actuator and the 3D-printed stage are precise enough, the RCM point is the center point, and the shoulder trajectory is a perfect ±14 degree circular arc with the stage's center point. Hence, in order to validate, the Euclidean distance between the detected RCM point (P_{in}) and the stage's center point is measured as an RCM-position detection error, and the difference in tangent

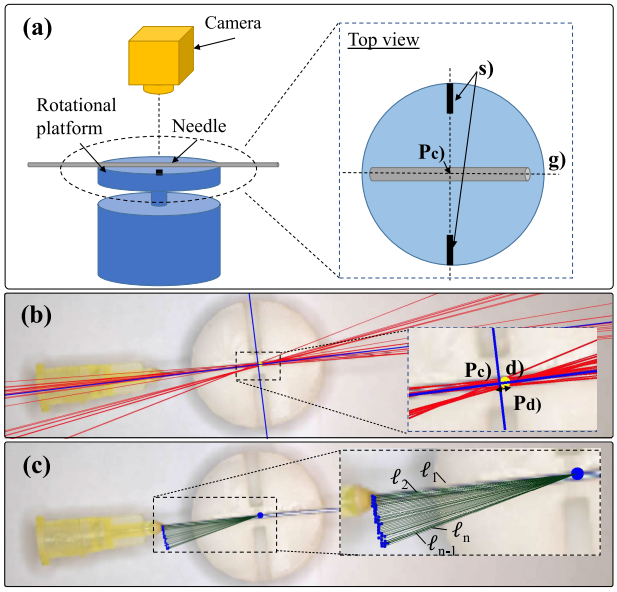

FIGURE 12. The validation setup. (a) presents the structure of the validation setup by using a calibrated camera, a 1-DoF platform with a groove (g), and slits (s) to indicate the center point (P_c). (b) shows the real result of RCM position detection validation. Red center lines mark the needle orientation during the rotation, and two blue lines represent the center point of the platform. (d) shows the distance between the center point (P_c) and the detected point (P_d). (c) shows the setup for calculating the distance between all detected shoulder trajectory points distances (l_n) from the detected center point to evaluate the radial deviation detection method.

TABLE 5. Average time measurements over 10 calibrations at every step of the pipeline in seconds. The movement refers to the overall time for 2-times symmetric RCM movement (± 6 degrees, and Calibration and re-initialize refer to the time for calculation/updating the parameters and putting the robot in the initialized mode respectively.

step	movement	III-B1	III-C	calibration	initialize
time(s)	166	0.183	0.314	0.270	52

line slope ($deg_{Dist(sh2rcm)}$) and 90 degrees is considered as RCM-deviation detection error. A 23 gauge needle (G-34285/ Geuder AG), with a diameter of 0.64 mm, is used. In this experiment, the RCM position and RCM radial detection accuracy are analyzed 0.144 mm and 0.29 degree separately (Fig. 12(b), (c)).

1) INFERENCE RATE

Performance measurements also give valuable insight into the usefulness of every method. In the mentioned 10-times calibration experiment (IV-F), the calibration process is split into several steps at run-time (Fig.2).

Each 2-times symmetric RCM movement in our robot takes 32 seconds, and on average, we need 2.6 times iteration to make the calibration done for each plane with criteria mentioned in IV-B1: Step3. Therefore, the RCM movement takes 224 seconds; meanwhile, all frames are extracted and processed in real time. With an interface of an Nvidia GeForce RTX A4000, Table. 5 shows the time measurements' results for each computation step (Fig.2). The results show

that the pipeline can tune the robot software in an average of 210 seconds.

V. DISCUSSION

It is worth noting that human surgeons naturally have an advantageous way of maintaining the RCM movement compared to robotic systems, and surgeons are able to flexibly adjust the force of the instrument manipulation by the haptic-visual feedback and the freedom to slightly mobilize the eye by exerting extrusion to the trocar. Moreover, RCM constraint in manual robotic surgery has more relaxed criteria because the robot is controlled by the surgeon based on haptic-visual feedback. For example for human surgeons, it is a clinical standard to keep the error of RCM position within 3 mm [10] when the instrument is introduced through the trocar. In contrast, surgical robots, at this stage, without human-level adaptability are naturally constrained by their mechanical design and hence have less freedom of movement. Considering this fact, with higher RCM positional error, robots may be limited in their effective working volume, even to the extent that surgical maneuvers can no longer be performed, and a robot with RCM redial deviation can not even move towards the target with needed micron precision. As a result, there is only little room for surgical robots to tolerate RCM errors, especially when they are amplified by the forward kinematics. Due to this fact, the imperative arises for pre-operative RCM kinematic calibration as an indispensable step. This crucial calibration process becomes necessary to ascertain that the RCM accuracy remains within a margin that is both safe and meets the specific requirements of the surgical application. This also explains why we manually set the positional RCM error tolerance in Section IV-B to 0.5 mm for our robotic system, instead of the less precise standard of 3 mm for human surgeons. Meanwhile, this high-precision constraint demands more iterations during parameter optimization and consequentially leads to a longer duration of the preoperative calibration. This also has implications for the eventual integration of surgical robots into operating rooms, as a balance between the precision and duration of preoperative calibration needs to be investigated.

VI. CONCLUSION

This paper proposes a preoperative vision-based RCM calibration method to compensate for the position error and radial deviation in the RCM mode through fine-tuning kinematic parameters. We validated our approach using a 5-DoF ophthalmic software-RCM robot. We showed that our strategy for kinematic decomposition and image-based RCM-related parameters evaluation in two decoupled working planes is consistent with the theoretical RCM analysis and succeeded in constraining the error of RCM position within the defined 0.50 mm. Furthermore, the tooltip accuracy is improved from 0.16 mm and 0.241mm to 0.085mm and 0.018mm in the XZ and XY planes, respectively. Additionally, we demonstrated the generalizability of our analysis method by applying it to analyze another conventional 6-DoF SRCM robot.

It should be pointed out that the accuracy of calibration hinges on various factors. Firstly, the quality of joint manufacturing and assembly plays a critical role. Since calibration involves intricate kinematic calculations, all joints are assumed to be meticulously manufactured and precisely assembled, particularly in delicate surgical procedures. Secondly, in vitreoretinal surgeries, the instruments are extremely small, often within the sub-millimeter range. Thus, the calibration's accuracy is influenced by the quality of instrument segmentation. The resolution of the optical camera and the accuracy of the U-Net-like neural network are crucial aspects that determine how well the system can identify and segment these small instruments. The method's core concept involves decomposing the robot's kinematics into two perpendicular planes. This approach enhances the reliability and robustness of the calibration process. However, this technique is most suitable for robots with kinematics that can be decomposed in this manner. Certain robots with unique designs might only partially support this decomposition. It is also important to acknowledge that while the proposed method excels at addressing geometric errors through the kinematic breakdown, it does not rectify non-geometric errors like backlash (play in joints) or misalignment during assembly. Relying on a segmentation model to identify and extract relevant information in each frame necessitates the utilization of a graphical processing unit (GPU) for efficiently processing each frame.

The promising results of our calibration method demonstrate a strong potential for its future integration into robotic surgical systems for ophthalmic surgical automation.

ACKNOWLEDGMENT

(Alireza Alikhani and Satoshi Inagaki contributed equally to this work.)

REFERENCES

[1] M. J. Gerber, M. Pettenkofer, and J.-P. Hubschman, "Advanced robotic surgical systems in ophthalmology," *Eye*, vol. 34, no. 9, pp. 1554–1562, Sep. 2020.

[2] E. Rahimy, J. Wilson, T.-C. Tsao, S. Schwartz, and J.-P. Hubschman, "Robot-assisted intraocular surgery: Development of the IRISS and feasibility studies in an animal model," *Eye*, vol. 27, no. 8, pp. 972–978, Aug. 2013.

[3] M. A. Nasseri, M. Eder, S. Nair, E. C. Dean, M. Maier, D. Zapp, C. P. Lohmann, and A. Knoll, "The introduction of a new robot for assistance in ophthalmic surgery," in *Proc. 35th Annu. Int. Conf. IEEE Eng. Med. Biol. Soc. (EMBC)*, Jul. 2013, pp. 5682–5685.

[4] A. Molaei, E. Abedloo, M. D. de Smet, S. Safi, M. Khorshidifar, H. Ahmadieh, M. A. Khosravi, and N. Daftarian, "Toward the art of robotic-assisted vitreoretinal surgery," *J. Ophthalmic Vis. Res.*, vol. 12, no. 2, p. 212, 2017.

[5] X. He, D. Roppenecker, D. Gierlach, M. Balicki, K. Olds, P. Gehlbach, J. Handa, R. Taylor, and I. Iordachita, "Toward clinically applicable steady-hand eye robot for vitreoretinal surgery," in *Proc. ASME Int. Mech. Eng. Congr. Expo.*, Nov. 2012, pp. 145–153.

[6] J. F. Arevalo, M. H. Berrocal, J. D. Arias, and T. Banaee, "Minimally invasive vitreoretinal surgery is sutureless vitrectomy the future of vitreoretinal surgery?" *J. Ophthalmic. Vis. Res.*, vol. 6, no. 2, pp. 136–141, 2011.

[7] J. T. Wilson, M. J. Gerber, S. W. Prince, C.-W. Chen, S. D. Schwartz, J.-P. Hubschman, and T.-C. Tsao, "Intraocular robotic interventional surgical system (IRISS): Mechanical design, evaluation, and master-slave manipulation," *Int. J. Med. Robot. Comput. Assist. Surg.*, vol. 14, no. 1, p. e1842, Feb. 2018.

[8] W. Wei, R. Goldman, N. Simaan, H. Fine, and S. Chang, "Design and theoretical evaluation of micro-surgical manipulators for orbital manipulation and intraocular dexterity," in *Proc. IEEE Int. Conf. Robot. Autom.*, Apr. 2007, pp. 3389–3395.

[9] A. Gijbels, K. Willekens, L. Esteveny, P. Stalmans, D. Reynaerts, and E. B. Van der Poorten, "Towards a clinically applicable robotic assistance system for retinal vein cannulation," in *Proc. 6th IEEE Int. Conf. Biomed. Robot. Biomechatronics (BioRob)*, Jun. 2016, pp. 284–291.

[10] T. Sakai, K. Harada, S. Tanaka, T. Ueta, Y. Noda, N. Sugita, and M. Mitsuishi, "Design and development of miniature parallel robot for eye surgery," in *Proc. 36th Annu. Int. Conf. IEEE Eng. Med. Biol. Soc.*, Aug. 2014, pp. 371–374.

[11] K. Faridpooya, S. H. M. van Romunde, S. S. Manning, J. C. van Meurs, G. J. L. Naus, M. J. Beelen, T. C. M. Meenink, J. Smit, and M. D. de Smet, "Randomised controlled trial on robot-assisted versus manual surgery for pucker peeling," *Clin. Experim. Ophthalmol.*, vol. 50, no. 9, pp. 1057–1064, Dec. 2022.

[12] S. Dehghani, M. Sommersperger, J. Yang, M. Salehi, B. Busam, K. Huang, P. Gehlbach, I. Iordachita, N. Navab, and M. A. Nasseri, "ColibriDoc: An eye-in-hand autonomous trocar docking system," in *Proc. Int. Conf. Robot. Autom. (ICRA)*, May 2022, pp. 7717–7723.

[13] J. Smits, D. Reynaerts, and E. V. Poorten, "Setup and method for remote center of motion positioning guidance during robot-assisted surgery," in *Proc. IEEE/RSJ Int. Conf. Intell. Robots Syst. (IROS)*, Nov. 2019, pp. 1315–1322.

[14] C. Gruijthuijsen, L. Dong, G. Morel, and E. V. Poorten, "Leveraging the fulcrum point in robotic minimally invasive surgery," *IEEE Robot. Autom. Lett.*, vol. 3, no. 3, pp. 2071–2078, Jul. 2018.

[15] L. Dong and G. Morel, "Robust trocar detection and localization during robot-assisted endoscopic surgery," in *Proc. IEEE Int. Conf. Robot. Autom. (ICRA)*, May 2016, pp. 4109–4114.

[16] A. Krupa, G. Morel, and M. de Mathelin, "Achieving high-precision laparoscopic manipulation through adaptive force control," *Adv. Robot.*, vol. 18, no. 9, pp. 905–926, Jan. 2004.

[17] B. Xiao, A. Alamdar, K. Song, A. Ebrahimi, P. Gehlbach, R. H. Taylor, and I. Iordachita, "Delta robot kinematic calibration for precise robot-assisted retinal surgery," in *Proc. Int. Symp. Med. Robot. (ISMR)*, Apr. 2022, pp. 1–7.

[18] M. Bai, M. Zhang, H. Zhang, L. Pang, J. Zhao, and C. Gao, "An error compensation method for surgical robot based on RCM mechanism," *IEEE Access*, vol. 9, pp. 140747–140758, 2021.

[19] Y. Tomiki, M. M. Marinho, Y. Kurose, K. Harada, and M. Mitsuishi, "On the use of general-purpose serial-link manipulators in eye surgery," in *Proc. 14th Int. Conf. Ubiquitous Robots Ambient Intell. (URAI)*, Jun. 2017, pp. 540–541.

[20] H. Suzuki and R. J. Wood, "Origami-inspired miniature manipulator for teleoperated microsurgery," *Nature Mach. Intell.*, vol. 2, no. 8, pp. 437–446, Jul. 2020.

[21] B. Rosa, C. Gruijthuijsen, B. Van Cleynenbreugel, J. V. Sloten, D. Reynaerts, and E. V. Poorten, "Estimation of optimal pivot point for remote center of motion alignment in surgery," *Int. J. Comput. Assist. Radiol. Surg.*, vol. 10, no. 2, pp. 205–215, Feb. 2015.

[22] J. T. Wilson, T.-C. Tsao, J.-P. Hubschman, and S. Schwartz, "Evaluating remote centers of motion for minimally invasive surgical robots by computer vision," in *Proc. IEEE/ASME Int. Conf. Adv. Intell. Mechatronics*, Jul. 2010, pp. 1413–1418.

[23] S. Marangoz, T. Zaenker, R. Menon and M. Bennewitz, "Fruit mapping with shape completion for autonomous crop monitoring," in *Proc. IEEE 18th Int. Conf. Automat. Sci. Eng. (CASE)*, Mexico City, Mexico, 2022, pp. 471–476, doi: 10.1109/CASE49997.2022.9926466.

[24] M. W. Spong, S. Hutchinson, and M. Vidyasagar, *Robot Modeling and Control*, vol. 3. New York, NY, USA: Wiley, 2006.

[25] H. Zhang, Q. Xia, J. Sun, and Q. Zhao, "A fully geometric approach for inverse kinematics of a six-degree-of-freedom robot arm," *J. Phys., Conf. Ser.*, vol. 2338, no. 1, Sep. 2022, Art. no. 012089.

[26] M. A. Nasseri, P. Gschirr, M. Eder, S. Nair, K. Kobuch, M. Maier, D. Zapp, C. Lohmann, and A. Knoll, "Virtual fixture control of a hybrid parallel-serial robot for assisting ophthalmic surgery: An experimental study," in *Proc. 5th IEEE RAS/EMBS Int. Conf. Biomed. Robot. Biomechatronics*, Aug. 2014, pp. 732–738.

[27] Z. Zhang, "A flexible new technique for camera calibration," *IEEE Trans. Pattern Anal. Mach. Intell.*, vol. 22, no. 11, pp. 1330–1334, Apr. 2000.

[28] O. Ronneberger, P. Fischer, and T. Brox, "U-Net: Convolutional networks for biomedical image segmentation," in *Proc. Int. Conf. Med. Image Comput. Comput.-Assist. Intervent.* Cham, Switzerland: Springer, 2015, pp. 234–241.

[29] P. J. Huber, "Robust methods of estimation of regression coefficients1," *Ser. Statist.*, vol. 8, no. 1, pp. 41–53, Jan. 1977.

[30] M. Kass, A. Witkin, and D. Terzopoulos, "Snakes: Active contour models," *Int. J. Comput. Vis.*, vol. 1, no. 4, pp. 321–331, Jan. 1988.

[31] J. Traa, "Least-squares intersection of lines," Univ. Illinois Urbana-Champaign (UIUC), Champaign, IL, USA, Tech. Rep., 2013.

[32] S. Libeskind, *Euclidean and Transformational Geometry: A Deductive Inquiry*. Sudbury, MA, USA: Jones & Bartlett Publishers, 2008.

[33] S. Arlinghaus, *Practical Handbook of Curve Fitting*. Boca Raton, FL, USA: CRC Press, 1994.

ALIREZA ALIKHANI (Graduate Student Member, IEEE) received the B.Sc. degree in communication systems engineering and the M.Sc. degree in electronics engineering from the University of Tehran, Iran, in 2014 and 2017, respectively. He is currently pursuing the Ph.D. degree with the Department of Experimental Medicine, Technische Universität München, Germany. His research interests include robotics, machine learning, image-guided robotics, and robot-guided surgery.

SATOSHI INAGAKI received the B.Sc. and M.Sc. degrees in engineering from the Department of Metallurgy and Ceramics Science, Tokyo Institute of Technology, Japan. He is currently pursuing the Ph.D. degree with the Department of Experimental Medicine, Technische Universität München. His research interest includes techniques for the analysis and design of surgical robotic systems.

JUNJIE YANG received the bachelor's and master's degrees from Sun Yat-sen University, China, under the supervision of Prof. Huang Kai. He is currently pursuing the Dr.rer.Nat degree with the Medical Autonomy and Precision Surgery (MAPS) Laboratory, Technische Universität München, Germany, with Dr.-Ing Ali Nasseri and Prof. Nassir Navab. His research interests include robotic medical autonomy and AI-driven therapies.

SHERVIN DEHGHANI (Graduate Student Member, IEEE) received the bachelor's degree in computer science from the Sharif University of Technology, in 2017, and the master's degree in informatics (computer vision and machine learning) from Technische Universität München (TUM), where he is currently pursuing the Ph.D. degree in image-guided robotics interventions. During the Ph.D. studies, he spent six months as a Visiting Scholar with the Laboratory for Computational Sensing and Robotics, Johns Hopkins University. He is also passionate about bridging the gap between cutting-edge computer vision advancements and their application in ophthalmic interventions.

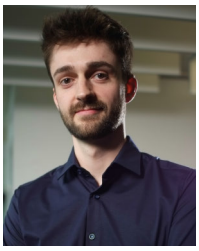

MICHAEL SOMMERSPERGER (Graduate Student Member, IEEE) received the B.Sc. degree in informatics and the M.Sc. degree in biomedical computing from Technische Universität München (TUM), in 2018 and 2021, respectively, where he is currently pursuing the Ph.D. degree with the Department of Informatics. From 2020 to 2021, he was a Visiting Scholar with the Laboratory for Computational Sensing and Robotics, Johns Hopkins University. His research interests include medical image visualization, computer graphics, and machine learning, primarily applied to ophthalmic interventions.

KAI HUANG (Member, IEEE) received the B.Sc. degree from Fudan University, China, in 1999, the M.Sc. degree from the University of Leiden, The Netherlands, in 2005, and the Ph.D. degree from ETH Zürich, Switzerland, in 2010. He was the Research Group Leader with Fortiss GmbH, Munich, Germany, in 2011, and a Senior Researcher with the Department of Computer Science, Technische Universität München (TUM), Munich, from 2012 to 2015. In 2015, he joined Sun Yat-sen University, China, as a Professor. He was appointed as the Director of the Institute of Cyber-Physical Systems, School of Data and Computer Science, in 2016. His research interests include techniques for the analysis, design, and optimization of embedded systems, particularly in the automotive domain. He was a recipient of the Best Paper Awards from ESTIMedia 2013 and SAMOS 2009 and the General Chairs' Recognition Award for Interactive Papers in CDC 2009.

MATHIAS MAIER was a Senior Physician with Augenklinik und Poliklinik, Klinikum rechts der Isar der Technische Universität München (TUM), from 1998 to 2001. After three years as a Partner and a Resident Doctor of the group practice Dr. Ober and Dr. Scharrer were involved in Fürth near Nuremberg. In August 2004, he returned to Klinikum rechts der Isar TUM and has been a Senior Consultant for the posterior sections of the eye ever since. He has also been the acting director of the eye clinic, since September 2021. He has many years of experience as a surgeon and is a specialist in retinal and vitreous surgery, and performs numerous operations in the eye clinic every day.

NASSIR NAVAB received the Ph.D. degree from INRIA, University of Paris XI, France. He studied mathematics and physics, computer engineering, and systems control. He then did two years of Postdoctoral Research with the MIT Media Laboratory, USA. Prior to becoming a Full Professor with Technische Universität München (TUM), in 2003, he was a Distinguished Member of the Technical Staff with Siemens Corporate Research (SCR), Princeton, NJ, USA. He has authored 100 scientific publications and has led more than 60 international patents. His research interests include computer-aided medical procedures, augmented reality, developing technologies to improve the quality of medical intervention, and bridging the gap between medicine and computer science. In 2006, he became a Board Member of MICCAI and an organizer of the world's leading conference on medical image computing and computer-assisted intervention. He is on the editorial board of many international journals, including IEEE TRANSACTIONS ON MEDICAL IMAGING, *MedIA*, and *Medical Physics*.

M. ALI NASSERI (Member, IEEE) received the joint Ph.D. degree in biomedical engineering from the School of Medical, Faculty of Mechanical Engineering, and the Faculty of Informatics, Technische Universität München (TUM), Munich, Germany, in 2015. He is currently the Head of the Medical Technology Laboratory, Department of Ophthalmology, Klinikum rechts der Isar, which is the university hospital of the TUM. He has coauthored more than 50 scientific publications, patents, and book chapters. His research interests include surgical robotics, medical imaging, machine learning, and the translation of these technologies to healthcare systems. He is an active member of ARVO and DOG.